Electronic Supplementary Material (ESI) for New Journal of Chemistry

Supporting Information

Mechanistic studies on the oxidative degradation of Orange II by peracetic acid catalyzed by simple manganese(II) salts. Tuning the lifetime of the catalyst

Sabine Rothbart, Erika E. Ember and Rudi van Eldik*

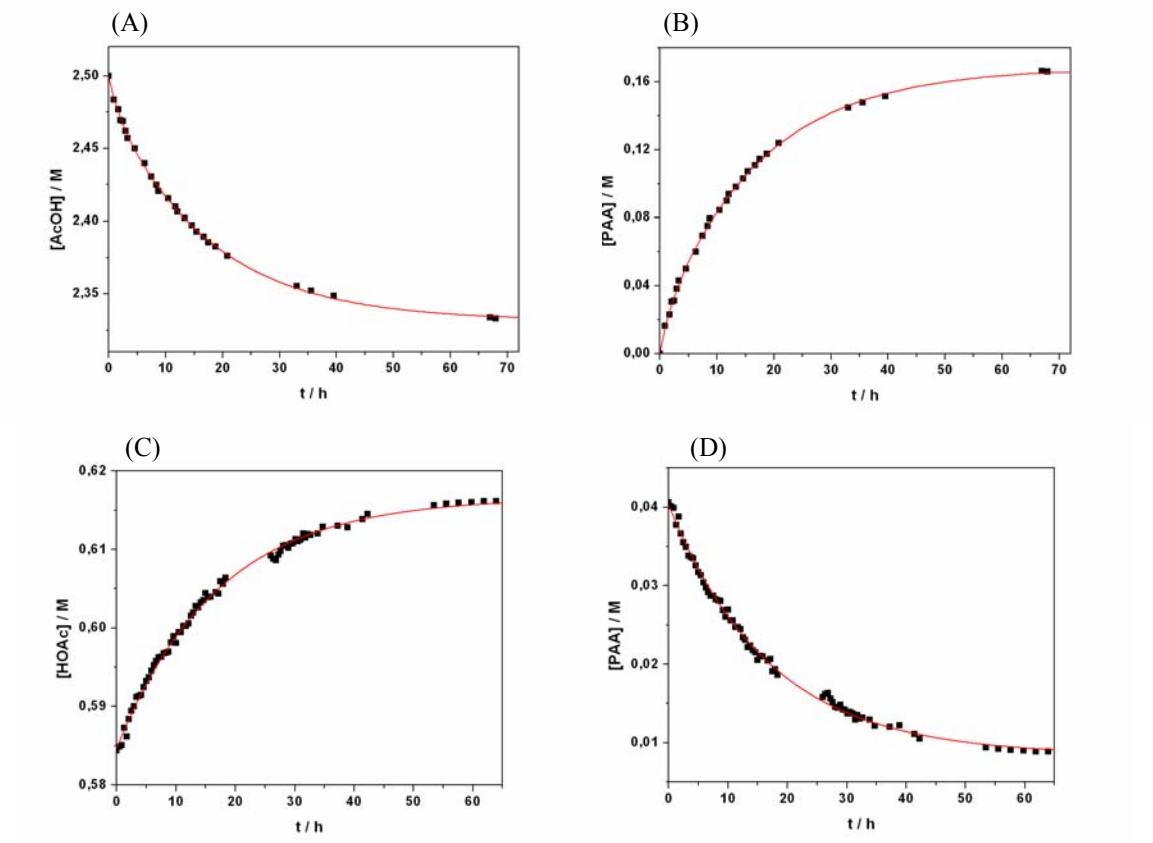

Figure S1. Time course for the consumption of AcOH (A) and the formation of PAA (B). Experimental conditions: 2.5 M AcOH, 2.5 M H_2O_2, 0.1 M H_2SO_4 and 25 °C. (C) Time course for the reformation of AcOH and the consumption of PAA (D). Experimental conditions: 0.041 M PAA (produced from 2.5 M AcOH, 2.5 M H_2O_2, 0.1 M H_2SO_4 at 25 °C), 0.1 M H_2SO_4 and 25 °C. The concentration profiles were calculated from the Lorenz fit of the ^{13}C-NMR signals at 179.2 ppm (CH_3-^{13}COOH) and 175.3 ppm (CH_3-^{13}C(O)OOH).

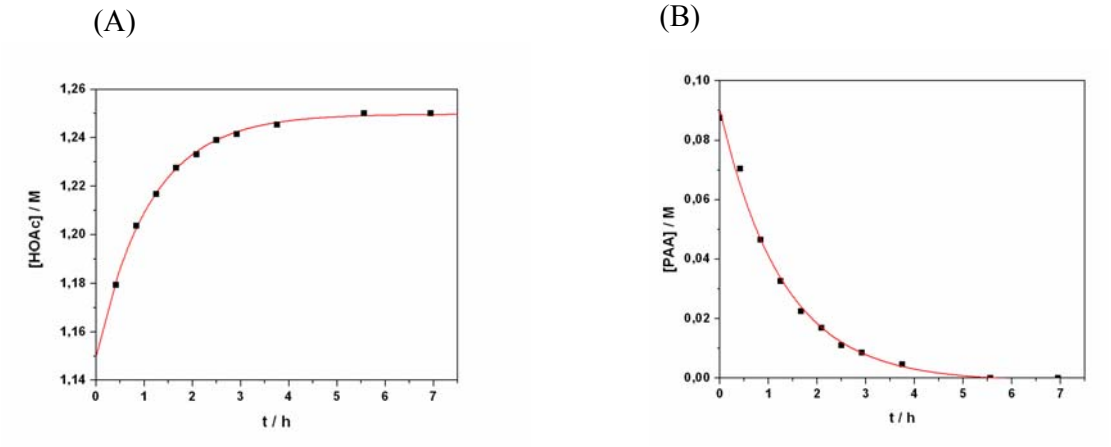

Figure S2. Time courses for the formation of AcOH (A) and decomposition of PAA (B) at pH ≈ 10 and 25 °C. The concentration profiles were calculated from the Lorenz fit of the ^{13}C-NMR signals at 179.2 ppm (CH_3-^{13}COOH) and 175.3 ppm (CH_3-^{13}C(O)OOH).

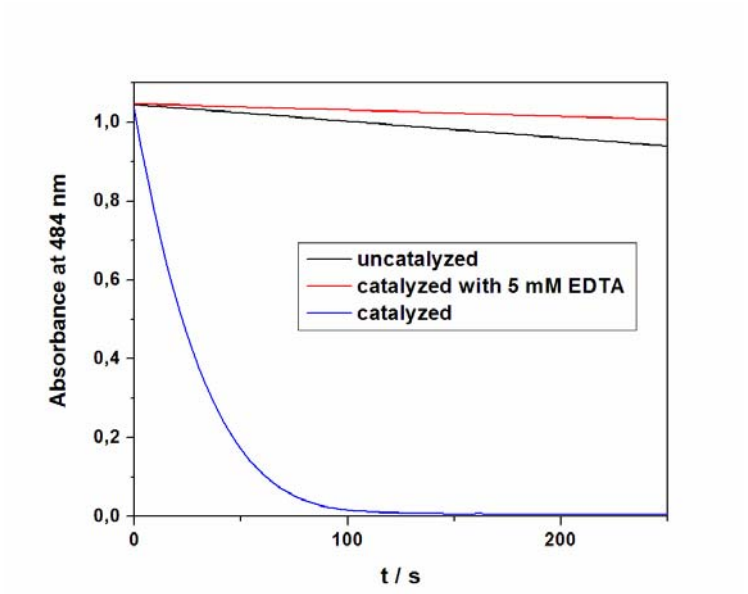

Figure S3. Comparison of the absorbance changes at 484 nm in the uncatalyzed reaction of 5 x 10^{-5} M Orange II with 5 mM PAA (—), with 5 mM PAA and 5 mM EDTA (—), and in the presence of 1 x 10^{-5} M Mn(II) catalyst (—). Reaction conditions: 0.05 M $NaHCO_3$ buffer, pH 9.50 and 25 °C.

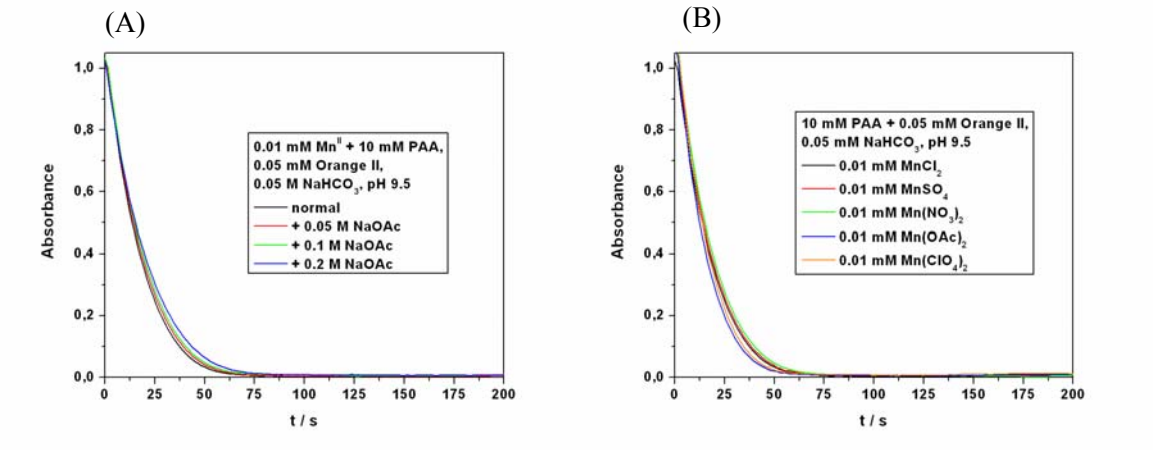

Figure S4. (A) Influence of acetate concentration on the reactivity of 1 x 10^{-5} M Mn(II) with 10 mM PAA and 5 x 10^{-5} M Orange in 0.05 M $NaHCO_3$ buffer at pH 9.5 and 25 °C. Absorbance change followed at 484 nm. (B) Comparison of different Mn(II) salts used as starting material for the catalytic decomposition of 5 x 10^{-5} M Orange II with 1 x 10^{-5} M Mn(II) and 10 mM PAA in 0.05 M $NaHCO_3$ buffer at pH 9.50 and 25 °C. Absorbance change followed at 484 nm.

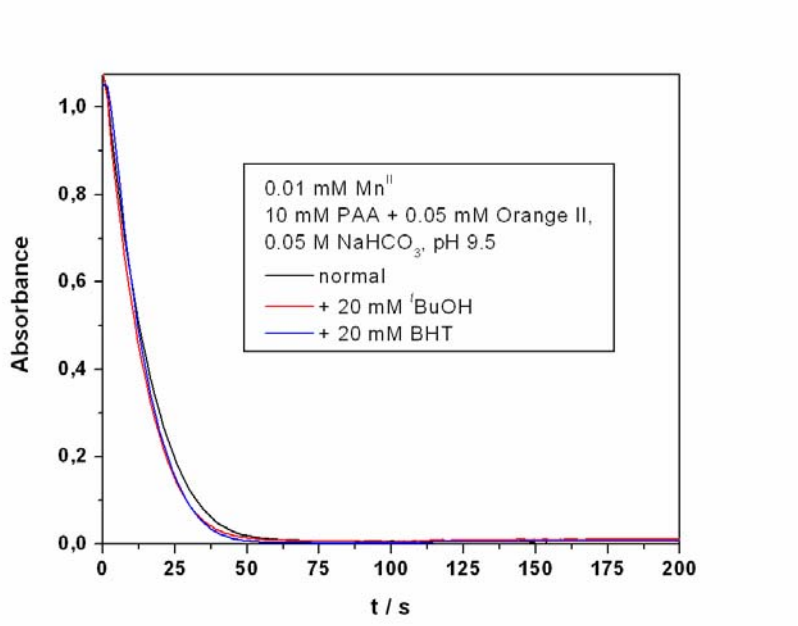

Figure S5. Comparison of the reactivity of 1 x 10^{-5} M Mn(II) with 10 mM PAA and 5 x 10^{-5} M Orange II in the absence (—) and presence of 20 mM ^{t}BuOH (—) and 20 mM BHT (—) as radical scavenger followed at 484 nm. Reaction conditions: 0.05 M $NaHCO_3$ buffer, pH 9.50 and 25 °C.

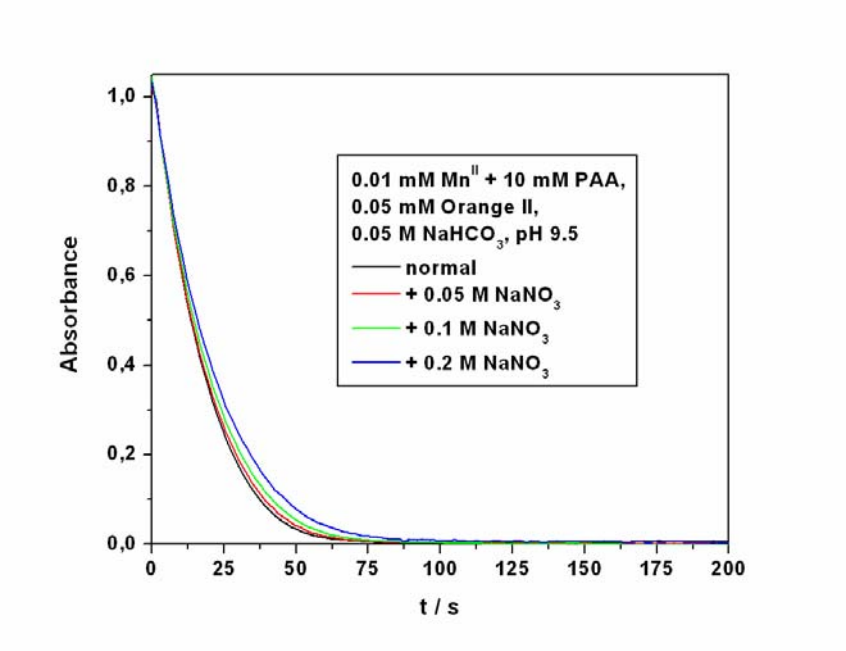

Figure S6. Effect of ionic strength (adjusted with different concentrations of $NaNO_3$) on the catalytic decomposition of 5 x 10^{-5} M Orange II with 1 x 10^{-5} M Mn(II) and 10 mM PAA in 0.05 M $NaHCO_3$ buffer at pH 9.50 and 25 °C. Absorbance change followed at 484 nm.

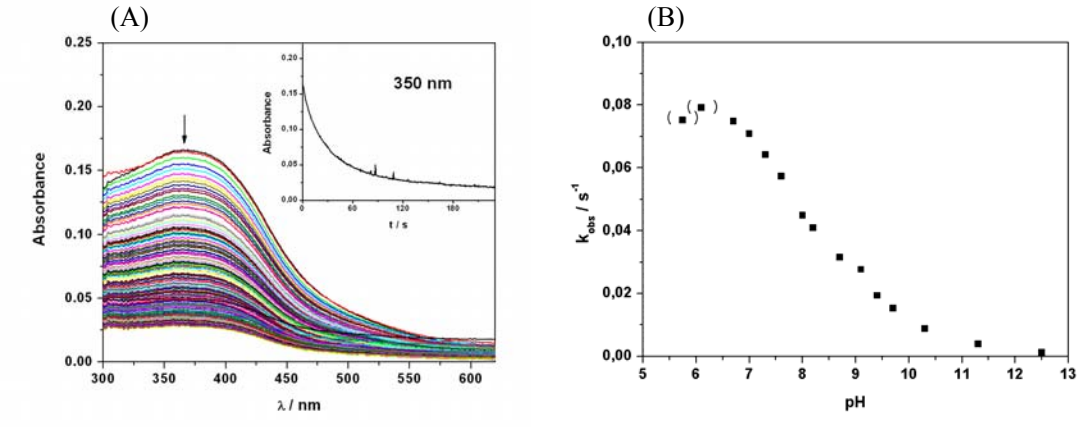

Figure S7. (A) UV/Vis spectral changes that accompany the reaction of 2 x 10^{-5} M colloidal MnO_2 with 2 mM H_2O_2 (0.05 M $NaHCO_3$ buffer) at pH 9.50 and 25 °C; inset: Absorbance changes at 350 nm; (B) Observed rate constants for the reduction of 2 x 10^{-5} colloidal M $Mn^{IV}O_2$ by 1 mM H_2O_2 followed at 350 nm. Reaction conditions: 0.05 M bicarbonate or phosphate buffer at 25 °C.

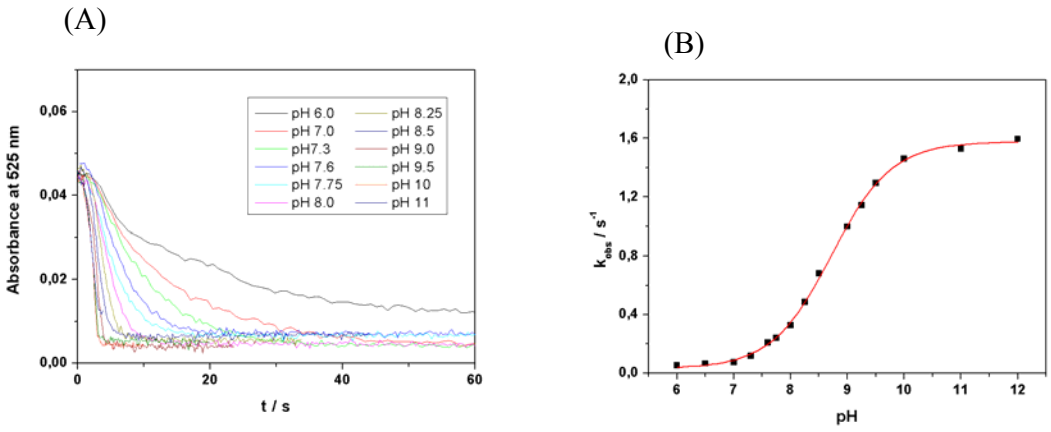

Figure S8. (A) Absorbance change at 525 nm for the reaction of 2 x 10^{-5} M $Mn^{VII}O_4^-$ with 5 x 10^{-4} M H_2O_2 as a function of pH. (B) Corresponding observed rate constants as a function of pH (induction period was neglected). Reaction conditions: stopped-flow experiments, 0.05 M bicarbonate or phosphate buffer at 25 °C.

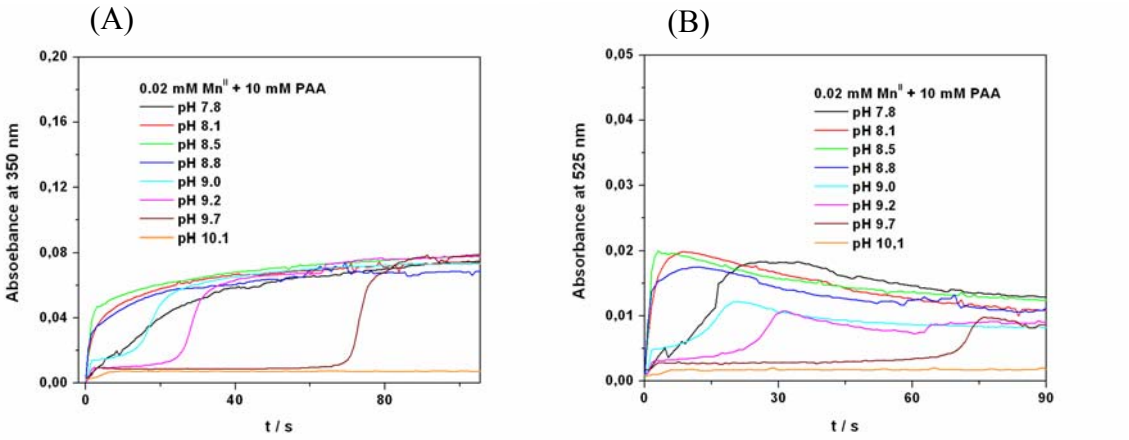

Figure S9. Absorbance changes at 350 nm (A) and 525 nm (B) for the reaction of 2 x 10^{-5} M Mn^{II} with 10 mM PAA in 0.05 M $NaHCO_3$ as a function of pH at 25 °C.

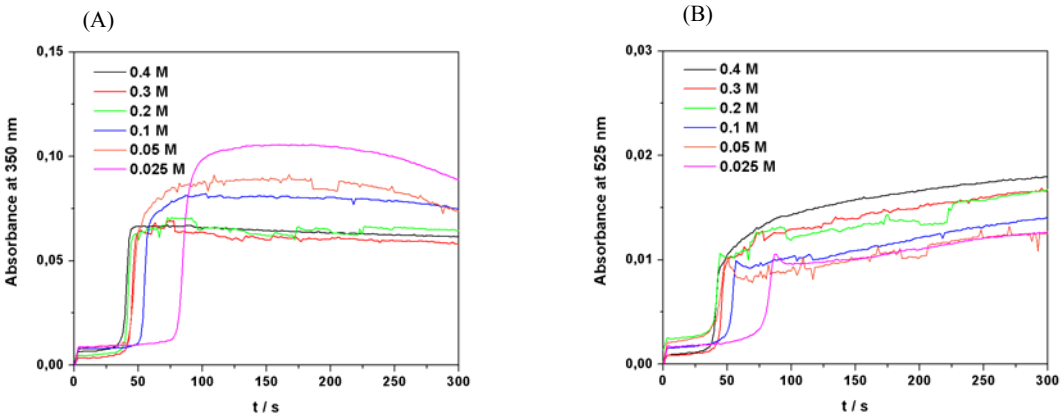

Figure S10. Absorbance changes at 350 nm (A) and 525 nm (B) for the reaction of 2 x 10^{-5} M Mn^{II} with 10 mM PAA at different total carbonate concentrations. Reaction conditions: pH 9.5 and 25 °C.

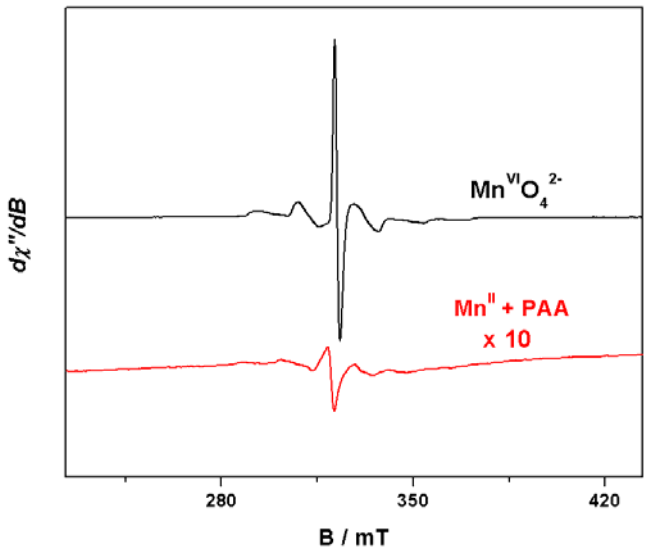

Figure S11. X-band EPR spectra recorded at 10 K for 1 x 10^{-4} M $Mn^{VI}O_4^{2-}$ in 10 M KOH (—) and for the first sample taken after mixing 1 x 10^{-4} M Mn^{II} with 25 mM PAA and 5 mM H_2O_2, 0.05 M carbonate buffer at pH 9.80 and 25 °C (—). EPR conditions: 8.95 GHz, 10 K, 1 mW microwave power, modulation amplitude 400 mT for (—) and 40 mT for (—).

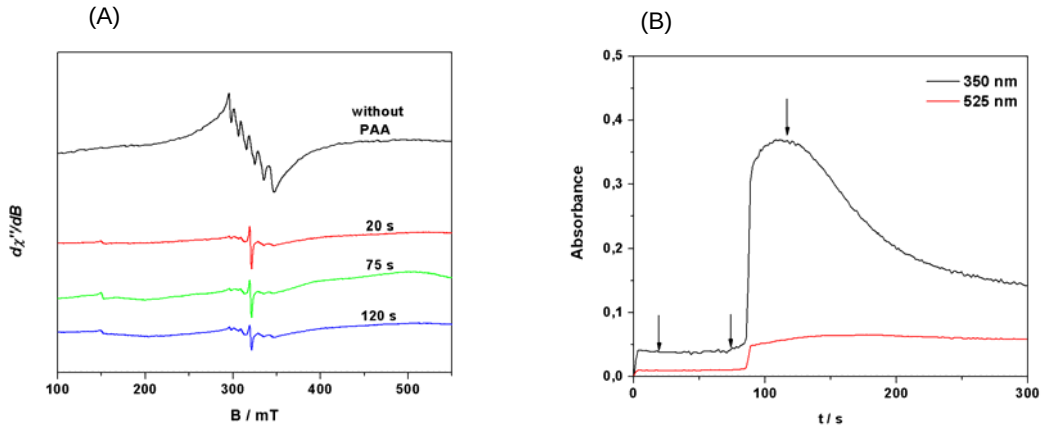

Figure S12. (A) X-band EPR spectra recorded at 10 K for 1 x 10^{-4} M Mn^{II} in carbonate buffer (—) and at different time intervals after the addition of 25 mM PAA and 5 mM H_2O_2 in 0.05 M $NaHCO_3$ with 20 % of ^{t}BuOH. (B) Kinetic traces at 350 and 525 nm; arrows mark the time at which different EPR samples were taken. Reaction conditions: 1 x 10^{-4} M Mn^{II} with 25 mM PAA and 5 mM H_2O_2 at pH 9.80 and 25 °C. EPR conditions: 8.95 GHz, 10 K, 1 mW microwave power, modulation amplitude 400 mT.

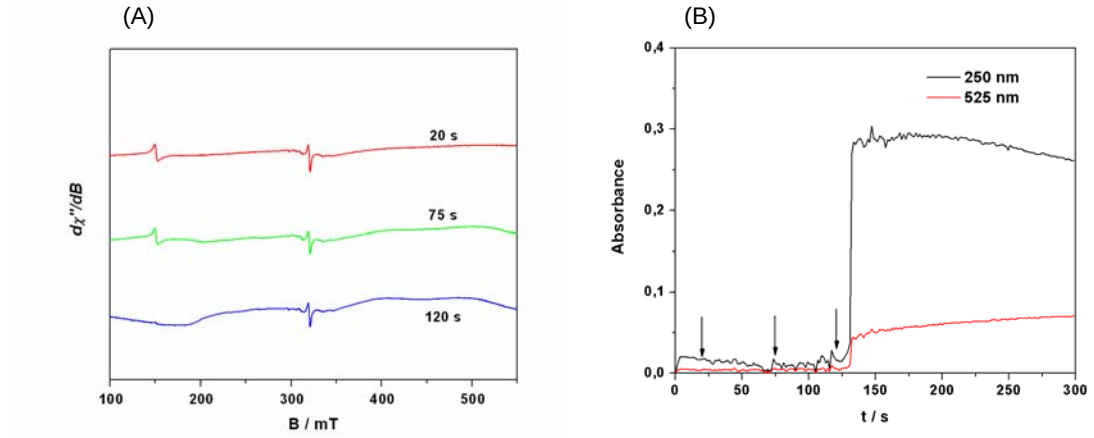

Figure S13. (A) X-band EPR spectra recorded at 10 K for 1 x 10^{-4} M Mn^{II} at different time intervals after the addition of 25 mM PAA and 5 mM H_2O_2 in 0.2 M carbonate buffer (B) Kinetic traces at 350 and 525 nm; arrows mark the time at which different EPR samples were taken. Reaction conditions: 1 x 10^{-4} M Mn^{II} with 25 mM PAA and 5 mM H_2O_2 at pH 9.80 and 25 °C. EPR conditions: 8.95 GHz, 10 K, 1 mW microwave power, modulation amplitude 400 mT.

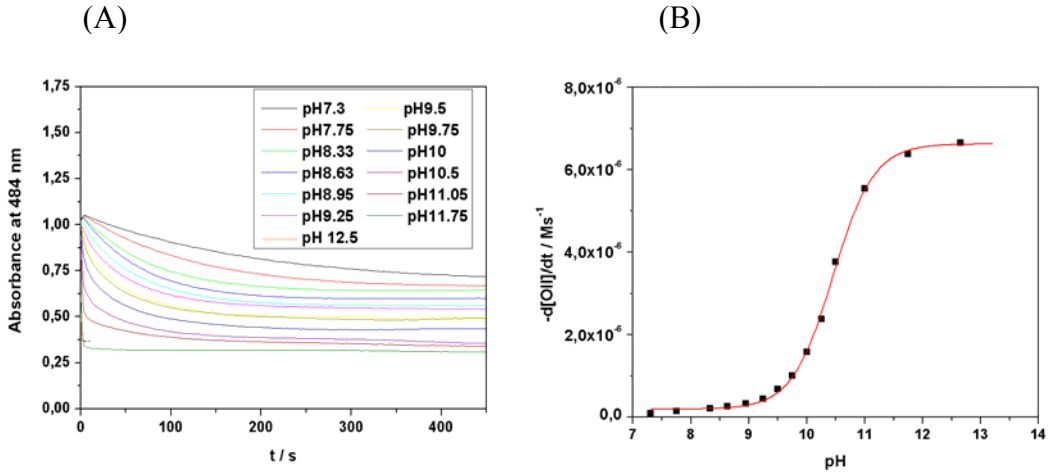

Figure S14. (A) Absorbance changes recorded at 484 nm for the reaction of 5 x 10^{-5} M $Mn^{VII}O_4^-$ with 5 x 10^{-5} M Orange II as a function of pH. (B) Initial rate as a function of pH. Reaction conditions: 0.05 M $NaHCO_3$ buffer and 25 °C.

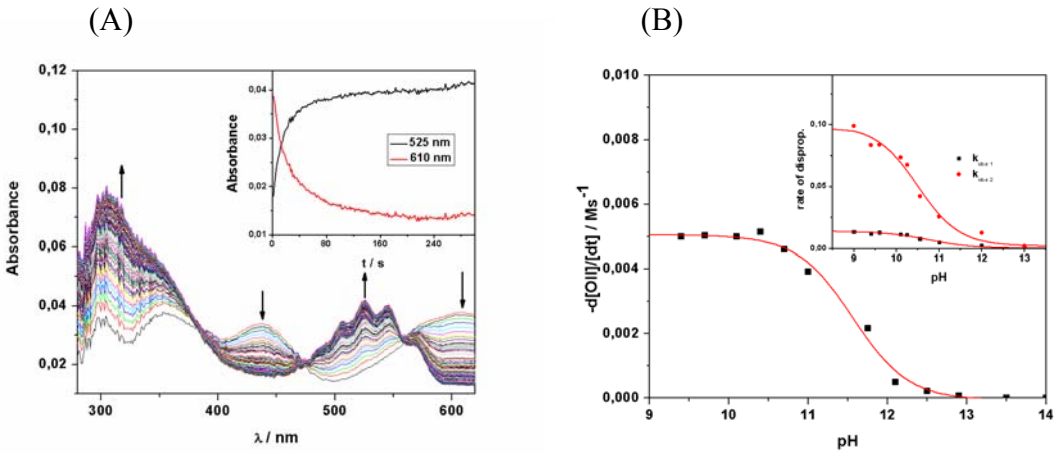

Figure S15. (A) UV/Vis spectral changes recorded for the disproportionation of 2 x 10^{-5} M $Mn^{VI}O_4^{2-}$. Inset: kinetic traces at 525 (—) and 610 nm (—). Reaction conditions: 0.05 M $NaHCO_3$ buffer, pH ~ 9.5 and 25 °C. (B) Initial rate of the reaction of 2 x 10^{-5} M $Mn^{VI}O_4^{2-}$ with 5 x 10^{-5} M Orange II as a function of pH. Inset: observed rate constants for the disproportionation of 2 x 10^{-5} M $Mn^{VI}O_4^{2-}$ as a function of pH; Reaction conditions: 2 x 10^{-5} M $Mn^{VI}O_4^{2-}$, 0.05 M $NaHCO_3$ buffer, 25 °C.

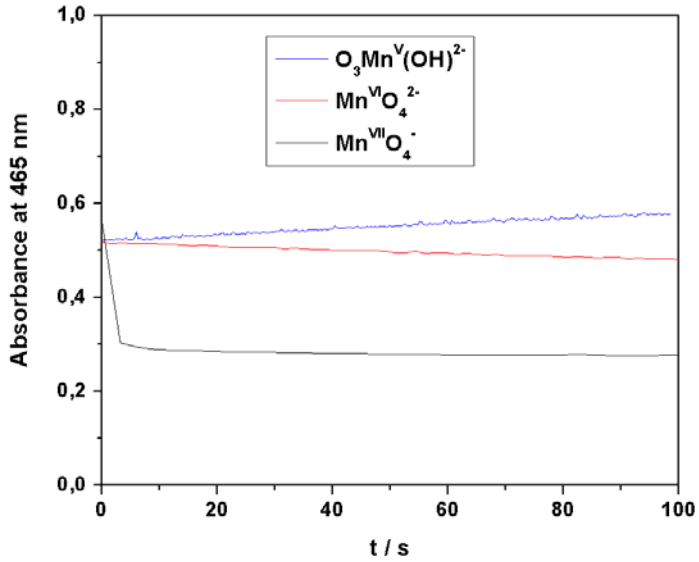

Figure S16. Comparison of the absorbance changes at 465 nm during the reaction of 5 x 10^{-5} M Orange II with 5 x 10^{-5} M $Mn^{VII}O_4^-$ (—), $Mn^{VI}O_4^{2-}$ (—) and $O_3Mn^{V}(OH)^{2-}$ (—) at pH 12.0. Reaction conditions: 0.05 M $NaHCO_3$ and 25 °C.

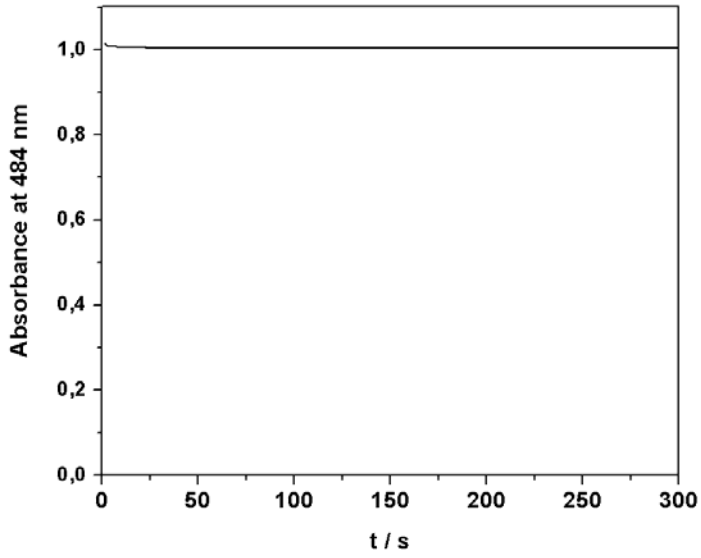

Figure S17. Absorbance change at 484 nm for the reaction of 1 x 10^{-5} M colloidal $Mn^{IV}O_2$ with 5 x 10^{-5} M Orange II. Reaction conditions: 0.05 M $NaHCO_3$ buffer, pH 9.50 and 25 °C.

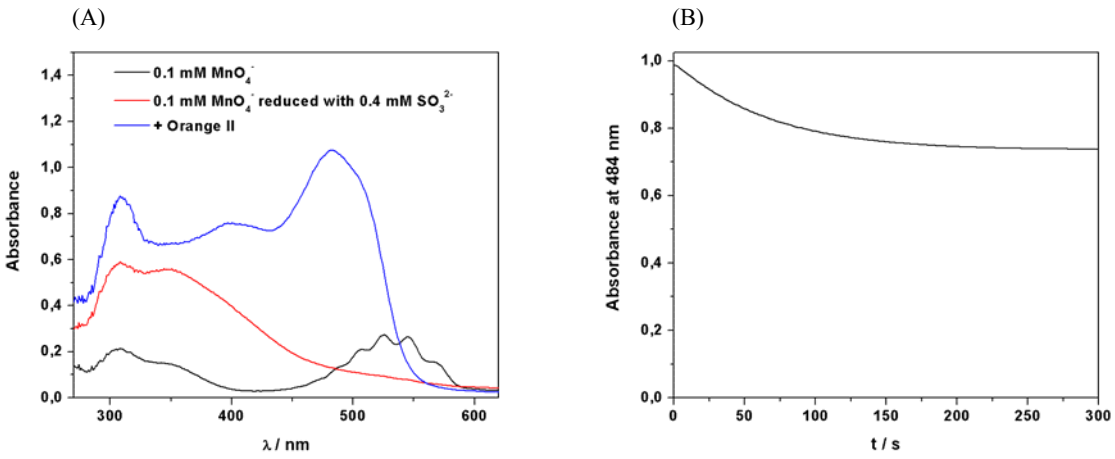

Figure S18. (A) UV/Vis spectra of 1 x 10^{-4} M MnO_4^- (—), 1 x 10^{-4} M MnO_4^- after the reduction by 4 x 10^{-4} M SO_3^{2-} (—) and immediately after addition of 5 x 10^{-5} M Orange II (—). (B) Absorbance changes at 484 nm that accompany the reaction of the in-situ generated Mn(IV) via reduction of MnO_4^-. Reaction conditions: 1 x 10^{-4} M MnO_4^-, 0.05 M $NaHCO_3$ buffer, pH 9.50 and 25 °C.

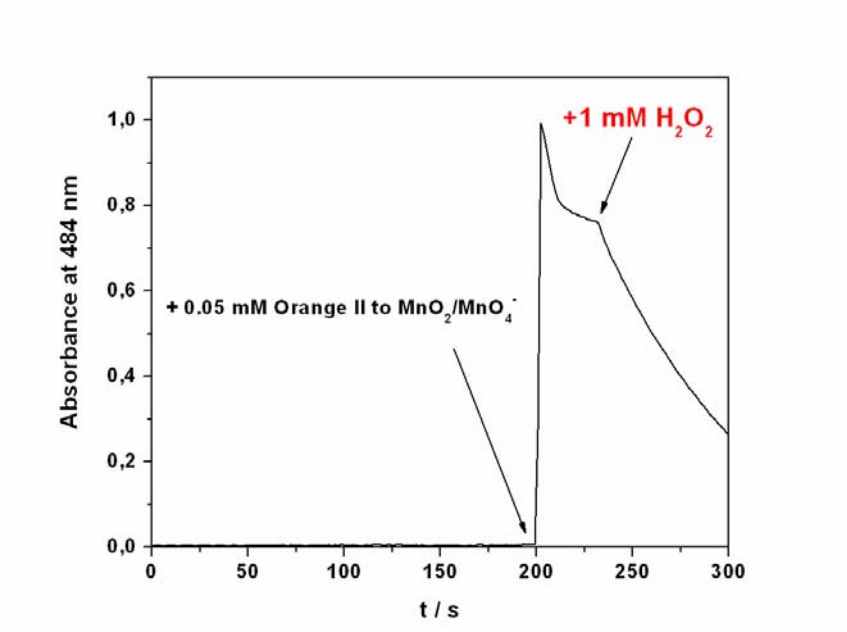

Figure S19. UV/Vis absorbance changes recorded at 484 nm showing the reactivation of the catalytic system by addition of 1 mM H_2O_2. Reaction conditions: 1 x 10^{-5} M Mn^{II}, 10 mM PAA, 5 x 10^{-5} M Orange II, 0.05 M $NaHCO_3$ buffer at pH 9.60 and 25 °C.

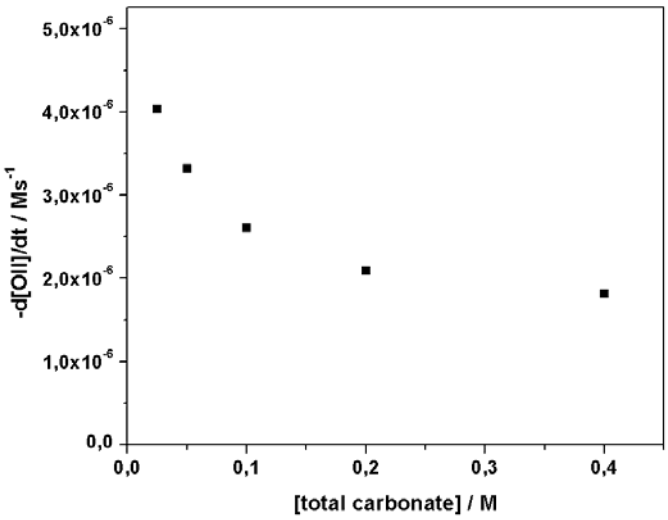

Figure S20. Dependence of the initial rate of the Mn(II) catalyzed degradation reaction on the total carbonate concentration. Reaction conditions: 1 x 10^{-5} M Mn^{II}, 0.01 M PAA, 5 x 10^{-5} M Orange II, 25 °C and pH 9.50.

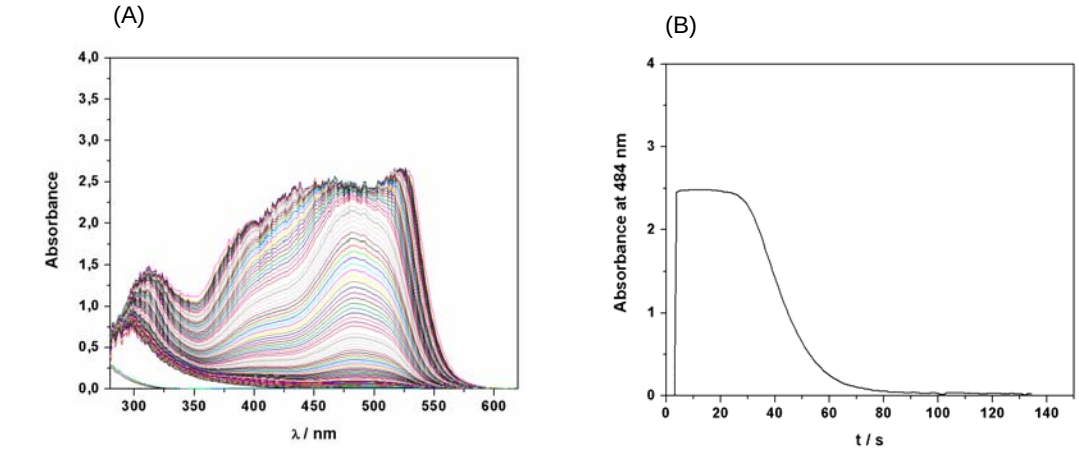

Figure S21. (A) UV/Vis spectral changes recorded during the reaction of 5 x 10^{-4} M Orange II with 0.025 M PAA catalyzed by 1 x 10^{-5} M Mn^{II}. (B) Corresponding absorbance *vs.* time plot at 484 nm. Reaction conditions: 0.05 M $NaHCO_3$ buffer at pH 9.50 and 25 °C (During the first 40 s of the measurement the absorbance remains above the detection limit of the detector due to the high Orange II concentration).

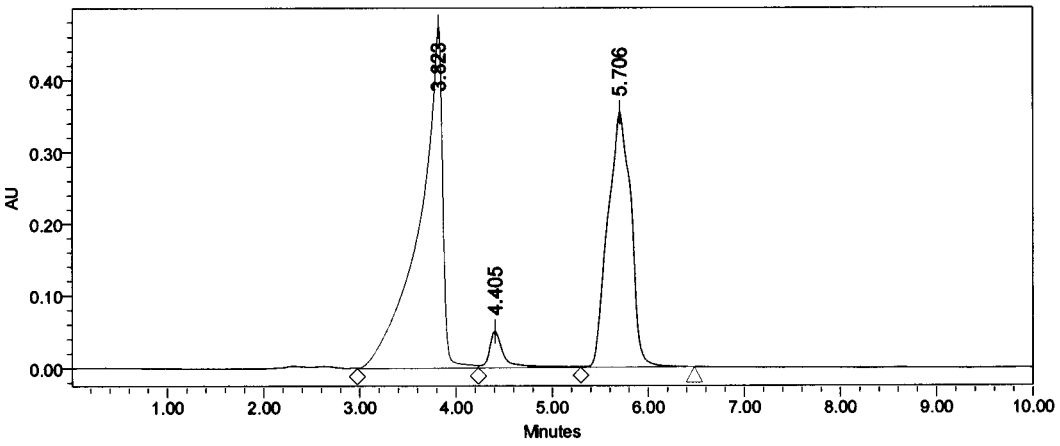

Figure S22. HPLC product analysis for the degradation of Orange II by PAA in the presence of Mn(II). Experimental conditions: 5 x 10^{-5} M Orange II, 1 x 10^{-5} M Mn^{II} and 10 mM PAA at pH 9.50 and 25 °C.

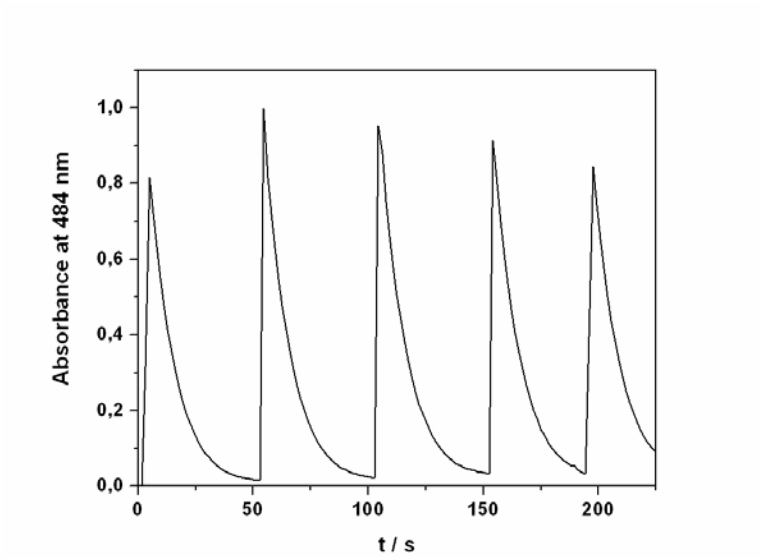

Figure S23. Absorbance *vs.* time traces at 484 nm for the oxidative degradation Orange II catalyzed by 1 x 10^{-5} M Mn^{II} and 10 mM PAA at pH 9.50 (0.05 M $NaHCO_3$ buffer) and 25 °C. Substrate addition was carried out in five consecutive steps each consisting of 5 x 10^{-5} M Orange II.

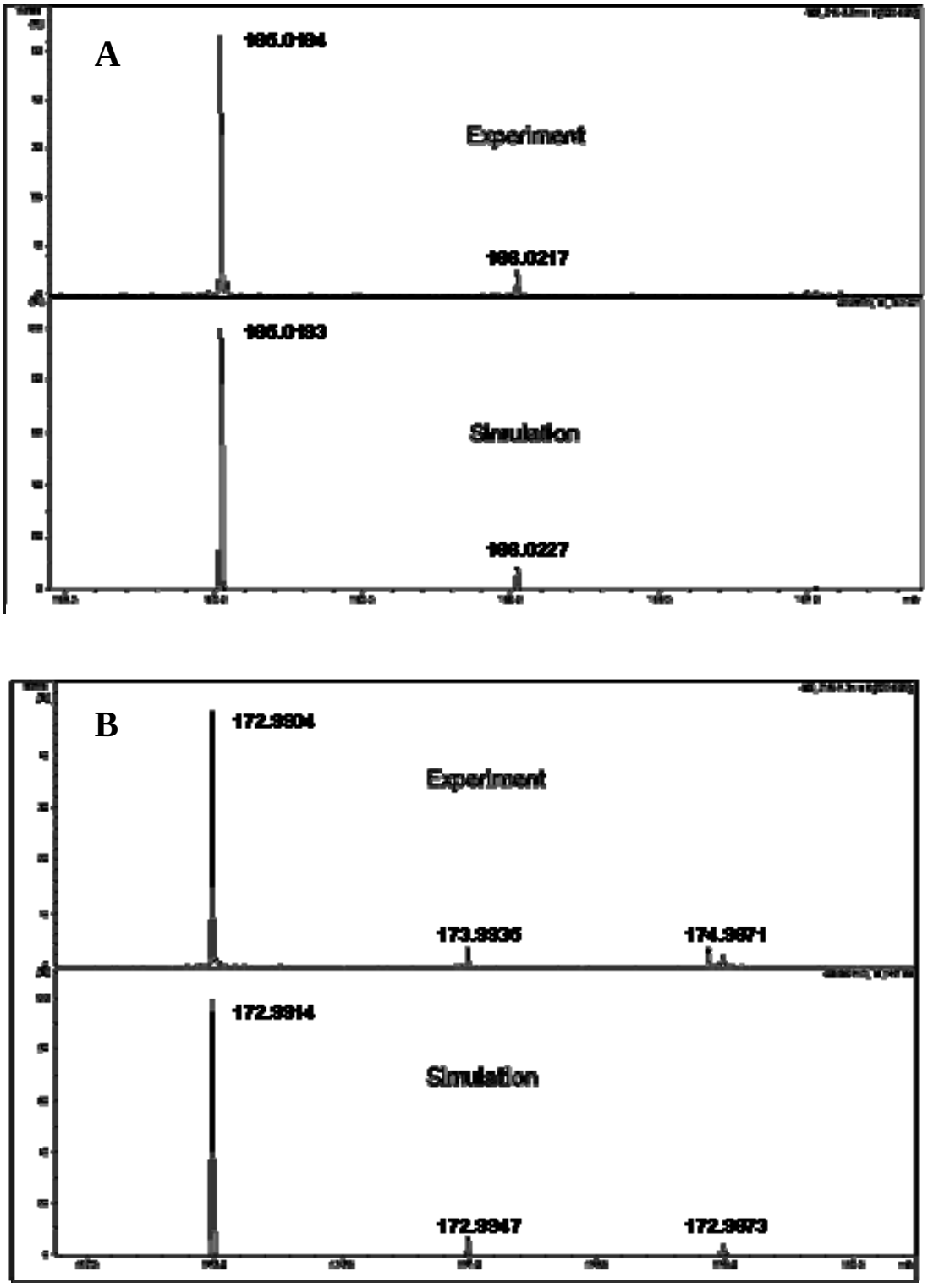

Figure S24. Mass spectra of mono-protonated phthalate (*m/z* = 165,0184) (A) and 4-hydroxybenzosulfonate (*m/z* = 172,9904) (B) as products of the degradation reaction in Figure S23.

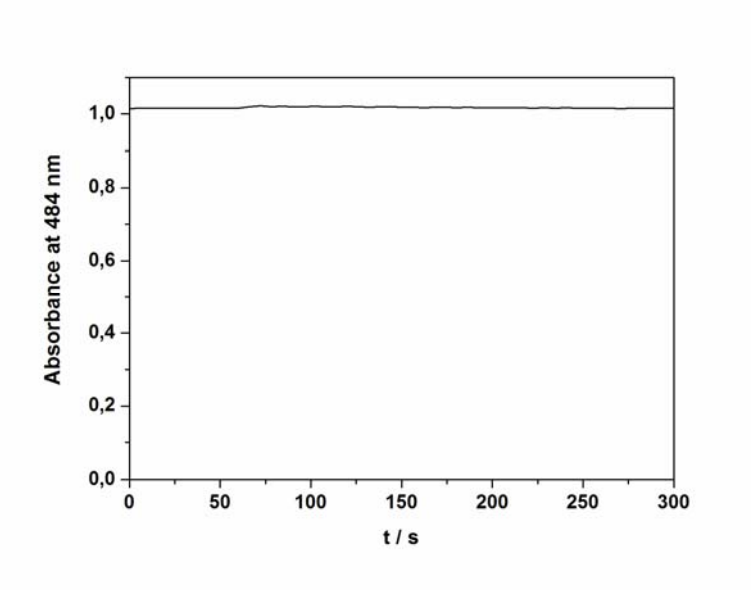

Figure S25. Absorbance changes at 484 nm in the reaction of 1 x 10^{-4} M $Mn^{III}(OAc)_3$ with 5 x 10^{-5} mM Orange II. Reaction conditions: 0.05 M $NaHCO_3$, pH 9.50 and 25 °C.

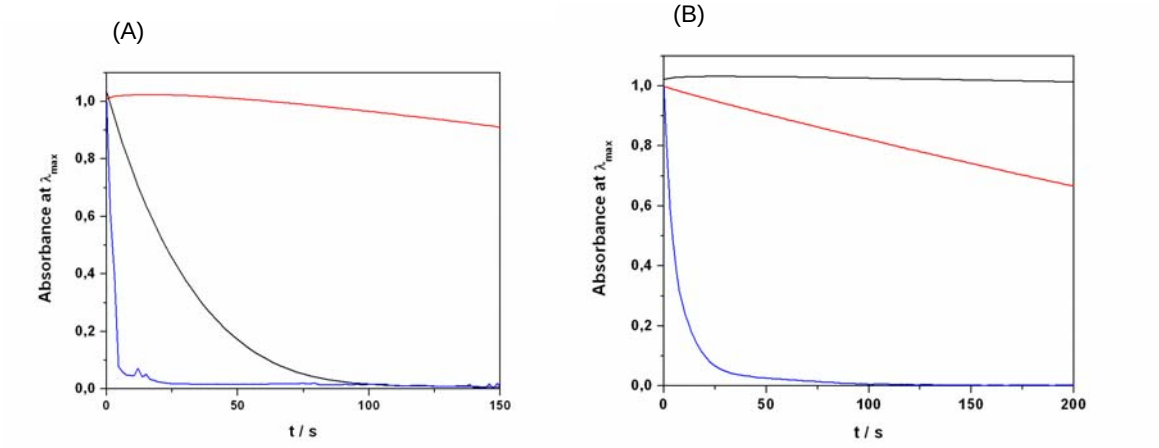

Figure S26. Comparison of the absorbance changes recorded at λ_{max} of the corresponding dye during the reaction of 5 x 10^{-5} M dye with 1 x 10^{-5} M Mn^{II} (A) and 1 x 10^{-6} M Mn^{II} (B), respectively, and 0.005 M PAA containing solution for Methyl Orange 465 nm (—), Orange II 484 nm (—) and Calmagite 612 nm (—). Reaction conditions: 0.05 M $NaHCO_3$, pH 9.50 and 25 °C.